Interparticle delivery and detection of volatile singlet oxygen at air/solid interfaces

Andrés M. Durantini[1,2,†,*] and Alexander Greer[1,2*]

[1] Department of Chemistry, Brooklyn College, Brooklyn, New York, USA

[2] Ph.D. Program in Chemistry, The Graduate Center of the City University of New York, New York, New York, USA

KEYWORDS: interfacial reactive oxygen, airborne singlet oxygen, total quenching rate constants, singlet oxygen quantum yields.

Table of Contents Graphic

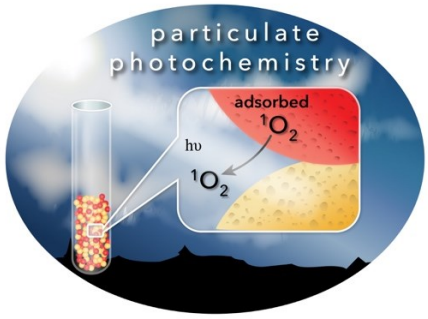

ABSTRACT: An interparticle system has been devised that allows airborne singlet oxygen to transfer between particle surfaces. Singlet oxygen is photogenerated on a sensitizer particle, where it then travels through-air to a second particle bearing an oxidizable compound—a particulate-based approach with some similarities to reactive oxygen quenching in the atmosphere. In atmospheric photochemistry, singlet oxygen is generated by natural particulate matter, but its formation and quenching between particles has until now not been determined. Determining how singlet oxygen reacts on a second surface is useful and was developed by a 3-phase system (particle-air-particle) *inter*particulate photoreaction with tunable quenching properties. We identify singlet oxygen quenching directly by near-IR phosphorescence in the airborne state and at the air/particle interface for total quenching rate constants (k_T) of adsorbed anthracene trapping agents. The air/solid interface k_T of singlet oxygen by anthracene-coated particles was $(2.8 \pm 0.8) \times 10^7$ g mol^{-1} s^{-1} for 9,10-dimethylanthracene and $(2.1 \pm 0.9) \times 10^7$ g mol^{-1} s^{-1} for 9,10-anthracene dipropionate dianion, and the lifetime of airborne singlet oxygen was measured to be 550 μs. These real-time interactions and particle-induced quenching steps open up new opportunities for singlet oxygen research of atmospheric and particulate processes.

INTRODUCTION

Airborne reactive oxygen species (ROS) are prominent in environmental photoreactions, and scientists have become interested in their reactions on surfaces. Such ROS, including $^1O_2$, $RO^\bullet$, $HO^\bullet$, and $O_2^{\bullet-}$ are commonly produced by sunlight irradiation via sensitized oxidation reactions.[1–11] Interactions of ROS can be significant in atmospheric and soil environments, such as on particulate matter (PM) and silicon dioxide.[12–15] However, they cannot be easily detected on surfaces using direct techniques, and are often limited to analysis by indirect techniques.

Using indirect techniques, a steady-state concentration of $^1O_2$ ($[^1O_2]_{ss}$) of $1.6 \pm 0.5 \times 10^{-12}$ M in fog was measured using furfuryl alcohol.[16,17] Indirect studies to deduce $[^1O_2]_{ss}$ have also been carried out on air/ice interfaces,[18] and on water surfaces.[19–21] The production of $^1O_2$ can arise from natural organic matter (NOM), in which their chromophores enable sensitization in water bodies exposed to sunlight.[5,19–23] Natural chromophores in soil can absorb light and by sensitization produce $^1O_2$.[2] Soil surface photooxidation was studied with $^1O_2$ traps agents, tetramethylethylene and 2,5-dimethylfuran[10] with sunlight exposure. Interestingly, airborne $^1O_2$ can diffuse up to 2 mm on soil.[9] In a historic experiment using a pressurized system, Kautsky conducted experiments in the 1930s mixing two sets of different size particles containing a photosensitizer (PS) (trypaflavine) and gaseous $^1O_2$ quencher (leucomalachite green) for early evidence of $^1O_2$.[24,25] Kautsky's experiment redesigned, Wolf et al. captured $^1O_2$ between two polymer surfaces,[26] Ruzzi et al. detected gaseous $^1O_2$ with a pressurized electron paramagnetic resonance (EPR) system,[27] and Naito et al.[28,29] used indirect single molecule fluorescence detection technique to show transport of $^1O_2$ between two surfaces via air (i.e., a solid/air/solid 3-

phase system). Studies using EPR technique have also shown that $^1O_2$ is also involved in photochemical air pollution.[2,30,31,32]

Such EPR and indirect trapping techniques can be limited in their utility as probes of $^1O_2$ at interfaces. Techniques that can directly track $^1O_2$ at interfaces by laser spectroscopy are needed to open the way to studying $^1O_2$ processes on particulates. Only a limited number of environmental studies have focused on direct $^1O_2$ detection. Recently, direct laser techniques to measure singlet oxygen quantum yields (Φ_Δ) by NOM sensitization by monitoring the $^1O_2$ phosphorescence directly[33] with Φ_Δ values of 0.6-3.8%.[6] Only limited number of studies have focused on solid-air-solid systems.[34–36] or how airborne $^1O_2$ interacts with natural and artificial surfaces.[9,11,37]

There are needs in terms of particulate environmental photochemistry, as there are difficulties in deducing the transport of ROS between surfaces. Direct laser work on heterogenous systems are more challenging than their solution-phase counterparts. Furthermore, it is not clear what surface effects are best suited for the generation and transfer of volatile ROS such as $^1O_2$. In the present study, we used an interparticle system for insight to how airborne $^1O_2$ transports from one surface to another and ways in which it is facilitated (Figure 1). Novel aspects of our work include advancing interfacial reactive oxygen chemistry with time-resolved air/solid $^1O_2$ direct laser work.

We hypothesized that a sensitizer particle (P_{PS}) will generate $^1O_2$ and the $^1O_2$ is delivered through-air to another particle bearing an oxidizable quencher (P_Q) in a 3-phase manner (particle-air-particle). The results demonstrate an interfacial $^1O_2$ production, where air/solid interface total quenching rate constants (*ASI-*k_T) and singlet oxygen quantum yields (Φ_Δ) are measured by direct phosphorescence via an interparticle method.

We report here a study of a 3-phase (particle-air-particle) system involving $^1O_2$. A mechanism which involves reaction of airborne $^1O_2$ with particle-adsorbed anthracene is proposed (Figure 2). This study provides the first direct evidence for a mechanism involving interfacial and airborne $^1O_2$. Porous Vycor glass (PVG) particles were coated with 8-acetoxymethyl-2,6-dibromo-1,3,5,7-tetramethyl pyrromethene fluoroborate (BODIPY, Br_2B-OAc) sensitizer (P_{PS}), which are irradiated with 532 nm light from a Nd:YAG laser. This BODIPY PS was chosen because it has increased photostability compared to its *bis*-iodinated analog I_2B-OAc or conventional sensitizers such as rose bengal.[38] The triplet excited state of the BODIPY PS on the particle is quenched by $^3O_2$ in an energy transfer process to generate $^1O_2$. The resulting $^1O_2$ phosphorescence was monitored at 1270 nm, which exhibited remarkably different lifetimes on the particles and as a free species in air. The quenching of $^1O_2$ arises on particles adsorbed with anthracene quenchers (P_Q). The particles P_Q were coated with quenching agents 9,10-anthracene dipropionate dianion (ADPD) or 9,10-dimethylanthracene (DMA), enabling *ASI*-k_T and Φ_Δ determinations. Our interparticle system offers a mechanistic tool to analyze $^1O_2$ migration through-air and its reaction at the air/solid interface of a second surface. There is novelty in the present air/particle and airborne $^1O_2$ laser work due to the lack of such direct measurements in the environmental chemistry literature. The work comprises of an interfacial air/solid and airborne $^1O_2$ detection system. The experimental data collected are consistent with the mechanism shown in Figure 2, as we describe below.

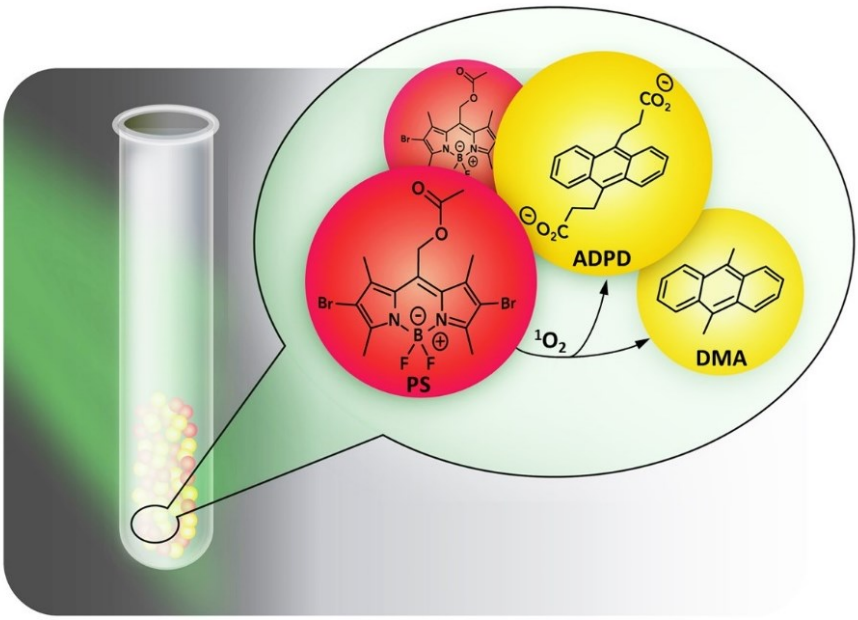

Figure 1. Interparticle transport of volatile $^1O_2$. Schematic showing the donor-acceptor interparticle $^1O_2$ migration system. Singlet oxygen diffuses through air after its generation on a photosensitizing donor particle (P_{PS}, BODIPY photosensitizer, red particles) and trapped on an acceptor particle (P_Q, anthracene quenchers DMA or ADPD, yellow particles).

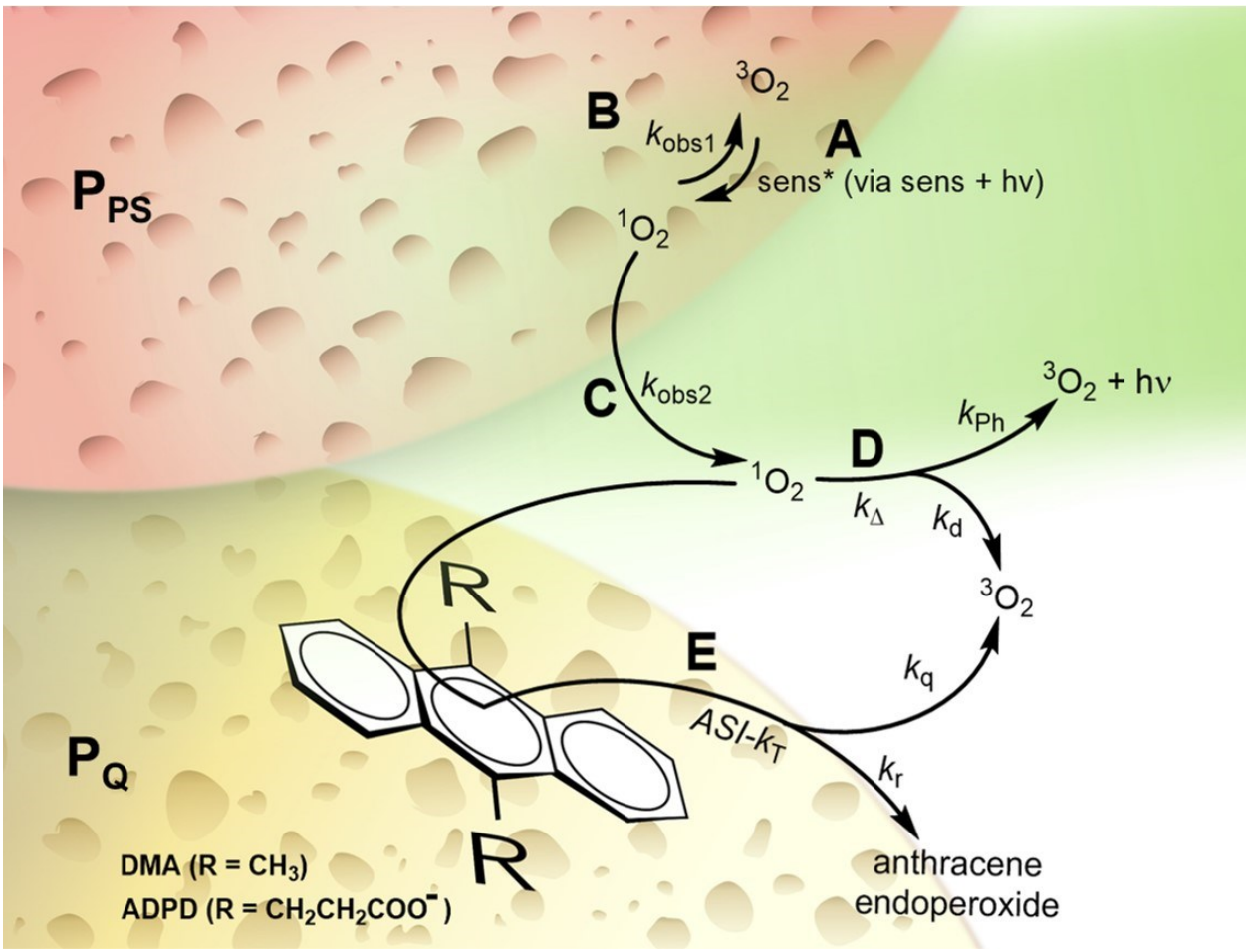

Figure 2. The interparticle reaction is a triphasic (particle-air-particle) system, which segregates a sensitizer particle from an acceptor particle for quenching of the generated airborne $^1O_2$. (A) Formation of $^1O_2$ by the excited photosensitizer particle (P_{PS}), (B) physical quenching of $^1O_2$ to $^3O_2$ (k_{obs1}) by the P_{PS} particle surface, (C) detection of airborne $^1O_2$ (k_{obs2}) in which (D) radiative and non-radiative deactivation of $^1O_2$ in air dominated by physical quenching and phosphorescence, and (E) reaction of $^1O_2$ with the anthracene trap on a separate particle (P_Q) to form an anthracene endoperoxide with $^1O_2$. Airborne $^1O_2$ can travel tenths of millimeter distances between P_{PS} to P_Q. There is no interparticle transfer of the sensitizer and anthracene traps.

MATERIALS AND METHODS

Materials and instrumentation. Corning 7930 porous Vycor glass (PVG), purchased from Advanced Glass and Ceramics, Holden, MA, was ground and sieved to particles (diameter 100-200 μm). PVG has a surface area of 250 m^2/g, it is a porous material with an average pore diameter of 4 nm.[42] Acetonitrile and dichloromethane were purchased from Sigma-Aldrich and used as received. Deionized water was purified using a U.S. Filter Corp. deionization system (Vineland, NJ, USA). UV−visible spectra were collected on an Agilent spectrophotometer.

Singlet oxygen phosphorescence at the air-solid interface and in air. The photosensitization of $^1O_2$ by the P_{PS} particles was demonstrated by measuring its phosphorescence upon irradiation of the sample with a Nd:YAG Q-switched laser producing 532 nm with a ~4 ns fwhm. The laser was operating at 5 Hz and 30 mJ/pulse, and 6 laser pulses were applied to acquire a trace. The $^1O_2$ phosphorescence was detected by a photomultiplier tube (H10330A-45 Hamamatsu Corp.) operating at a voltage of −650 V through a NIR bandpass filter centered at 1270 nm (OD4 blocking, fwhm = 15 nm). The signals were registered on a 600 MHz oscilloscope and the kinetic data for all the samples containing the PS were fitted with a biexponential function. An open quartz cuvette with a 10 mm path length containing 100 mg of P_{PS} or 100 mg of P_{PS} + 100 mg of P_Q particles was irradiated from the top reflecting the laser beam on a right-angle prism. Samples were purged with N_2 or air using a septum screw-capped quartz cuvette and were irradiated from the bottom by reflecting the laser beam. For the Φ_Δ measurements, the frequency was increased to 10 Hz and the power decreased to 10 mJ/pulse to avoid rapid photobleaching of the dye also, the signal of 3 laser pulses were averaged to acquire a trace. Further detail on the apparatus design is provided in the Supporting Information. Here,

apparatus dosing and optimization permitted to increase excitation power and the time resolution due to 6 order of magnitude increase in surface area.

Design of airborne $^1O_2$ quenching system at air/solid interfaces. Particles containing the Br_2B-OAc PS were prepared as described in the Supporting Information. The PS loading was 0.050 μmol/g of PVG particles. Stock solutions of the quenchers were prepared in H_2O (pH = 10) for ADPD and in acetonitrile for DMA. Different volumes of the quenchers were added in 5 vials containing 200 mg of particles to achieve the desired loading. The solvents were removed under vacuum in a rotary evaporator operating at 50 mbar and the samples were dried in the oven with reduced pressure for 1 h at 60 °C. To acquire the trace corresponding to the decay of $^1O_2$ phosphorescence, 100 mg of P_{PS} was mixed with 100 mg of P_Q containing the desired quencher and loading.

RESULTS AND DISCUSSION

"Lightening up" singlet oxygen for transport between particles. We sought an optimal $^1O_2$ photogeneration by the PS particles to allow a view of the through-space $^1O_2$ process. In a previous study,[34] we were not able to obtain direct lifetime measurements for airborne $^1O_2$ generated on a superhydrophobic surface embedded with a phthalocyanine particles. On that occasion, due to low phosphorescence emission, time resolution was not possible and only variations in the intensity were monitored. Here, we varied PS loading with emission and absorbance of Br_2B-OAc molecules (Figure S1, Supporting Information) that overlap by ~30% to avoid close proximity from high loading, <50 nm, where photoexcited sensitizer self-quenches by Föster resonance energy transfer (FRET).[39-41] Low PS loading is also undesirable due to low signal to noise ratios. Both under- and over-loading of PS will lead to less triplet excited states and thus less airborne $^1O_2$. A loading of 0.050 μmol of PS per gram of particle (μmol/g) was

found to be the optimal amount of PS adsorbed on the glass surface. The distance between PS molecules under these conditions was calculated to be 180 nm. Another consideration is that the PS remains embedded within the pores. Under this circumstance, the surface area is reduced to 70 m^2/g and the PS-PS distance to 94 nm. The average distance between PS molecules was calculated by estimating the area occupied by the molecule (Figure S2) relative to the surface area of particle. Based on these calculations, we predict that an optimal PS loading is 0.050 μmol/g for a compromise to maximize $^1O_2$ formation due to sufficiently high PS amounts, and yet minimize unwanted PS/PS self-quenching by FRET.

This was tested experimentally. Figure 3A shows the $^1O_2$ phosphorescence decay curves for 100 mg of P_{PS} with different PS loadings and the controls (native particles and $P_{non\text{-}PS}$ loaded with 0.050 μmol/g of H_2B-OAc, which gives no $^1O_2$ production). Fitting of the intensity vs time with a bi-exponential function (eq S1, Supporting Information) led to two distinct lifetimes (Figure 3B). The data in Table 1 support the identification of two lifetimes: a short lifetime (τ_{obs1}) of ~54 μs that remained similar at various PS loadings (entries 1-5), and a longer lifetime (τ_{obs2}) that varies with the amount of PS loading and reaches a maximum of ~540 μs (loading 0.050 μmol/g). A mono-exponential decay from background was observed, τ_{bckgrd} = ~35 μs, but this was not due to $^1O_2$ phosphorescence (eq S2, Supporting Information). This background signal corresponds to spurious light reaching the detector even when a NIR bandpass filter centered at 1270 nm was applied. The τ_{bckgrd} values showed very small variation among the different experiments bearing an experimental error of 1.0 μs. This background signal was verified not to be from $^1O_2$ phosphorescence by exciting native particles with constant laser power and varying the diameter of the NIR detector iris causing some light to reach the detector (Figure S3). Were the signal due to $^1O_2$, the signal intensity would have varied and the lifetime

would have remained essentially constant. Figure 3A and 3B show conditions that led to enhanced signal to get the best $^1O_2$ signal to background ratio. With this data in hand, a lifetime τ_1 is attributed to adsorbed $^1O_2$ and is the difference between τ_{obs1} and $\tau_{control}$ for native particles (Table 1). As we will see next, the long lifetime is attributable to airborne $^1O_2$.

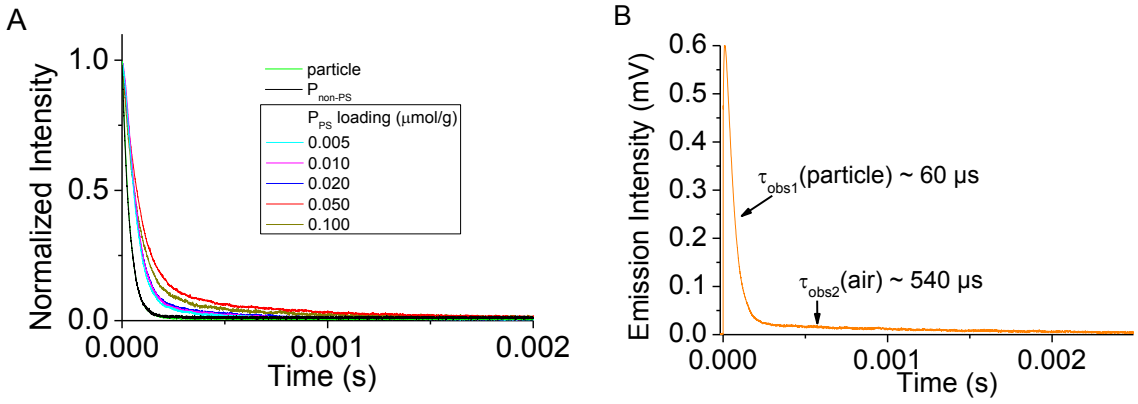

Figure 3. (A) Airborne $^1O_2$ decay curves photosensitized by P_{PS} particles loaded with varying amounts of photosensitizer (PS) (0.005-0.1 μmol/g particle). The decay curves for the native (uncoated) particles and the "non-photosensitizer" coated particle $P_{non\text{-}PS}$ (0.050 μmol/g particle) are also shown. (B) Decay curve showing the two $^1O_2$ lifetimes (τ_{obs1} and τ_{obs2}) from the bi-exponential fitting of the data for the interparticle $^1O_2$ exchange system. Intensity decay was monitored at 1270 nm.

Table 1. Singlet oxygen lifetimes obtained from the intensity decays curves for the controls and different particle loadings of the PS.

entry	PS loading (μmol sens/g particle)	τ_{obs1} (μs)[b]	τ_1 (μs)[b]	τ_{obs2} (μs)[b]
1[a]	0.005	50.3	15.2	373
2[a]	0.010	52.1	17.0	426
3[a]	0.020	53.5	18.4	432
4[a]	0.050	58.5	23.4	537
5[a]	0.100	55.2	20.2	416

[a] Particles coated with the sensitizer Br_2B-OAc. [b] Errors for the short lifetimes are ±1 μs and for the long lifetimes ±5-10 μs, and the error ranges for fitting were 0.01-0.03 μs. Values for τ_{bckgrd} are 35.1 and 34.8 μs for native particles and $P_{non\text{-}PS}$, respectively.

The $^1O_2$ particulate quenching connection. Direct detection reveals two lifetimes attributable to particle adsorbed $^1O_2$ and airborne $^1O_2$ (Table 2). Our experiments were carried out in the presence of air, and by sparging with N_2. Sparging with N_2 for 15 min a 100 mg of P_{PS}, as seen in Figure 4, led to a disappearance of the long lifetime component with only the short lifetime remaining (τ_{obs1} = 65.9 μs), where this value in entry 2 is due to trace O_2 remaining adsorbed to

191 the particle.[43] The slightly higher value 65.9 μs compare to the ~60 μs for P_{PS} (Table 2, entry 2)
192 in ambient conditions can be attributed to a reduction of humidity after purging with the inert
193 gas. After 15 min re-oxygenation of the particles with flowing air, the two lifetimes were
194 recovered (Table 2, entry 3). On the other hand, τ_{obs1} and τ_{obs2} reduced or disappeared (entry 4)
195 due to adsorbed water molecules, where $^1O_2$ is readily quenched. Indeed, we find that τ_1 = 3.8 μs
196 (Table 2, entry 4), which matches the known lifetime of $^1O_2$ in water.[35,44] An experiment was
197 carried out by incorporating quenchers to the particles. The phosphorescence signal was
198 analyzed with the addition of ADPD (Figure 1), a water-soluble anthracene derivative. Singlet
199 oxygen reacts with anthracenes to give endoperoxides.[45–47] The addition of P_{PS} coated with
200 ADPD (20 mg) resulted again in the loss of τ_{obs2} (Table 2, entry 5). The τ_1 was ~5 μs lower
201 respect to P_{PS} with a value of 19.2 μs indicating that the native particles deactivate $^1O_2$ only to a
202 minor extent.
203

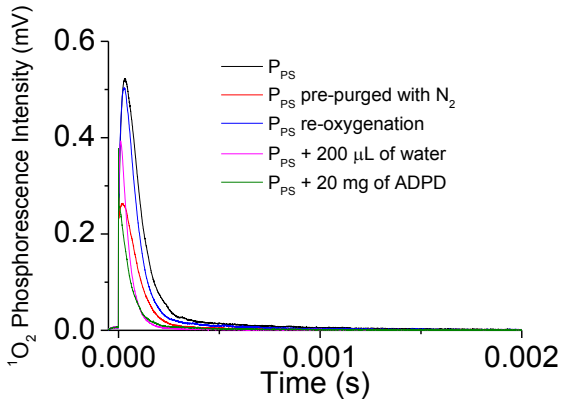

Figure 4. Airborne $^1O_2$ decay monitored upon photoexcitation of P_{PS} particles in the presence of different quenchers. The loading was 0.050 μmol ADPD per gram particle, and the intensity decay was monitored at 1270 nm.

Table 2. Singlet oxygen lifetimes from the 1270 nm intensity decays curves under various conditions.

entry	**condition**	**τ_{obs1} (μs)**[b]	**τ_1 (μs)**[b]	**τ_{obs2} (μs)**[b]
1[a]	-	61.2	24.8	560
2	pre-purge with N_2	65.9	29.5	-
3	re-oxygenation	58.1	21.7	475
4	200 μL H_2O	40.2	3.8	-
5	20 mg ADPD	55.7	19.3	-

[a] P_{PS} particles under ambient conditions. [b] Errors for the short lifetimes are typically ±1 μs and for the long lifetimes ±5-10 μs. The fitting errors range from 0.01 to 0.03 μs. The value for τ_{bckgrd} is 36.4 μs for native particles.

Interparticle control of airborne $^1O_2$ reactions. Next, control reactions were carried out to test the possibility of whether the donor and the acceptor migrate between particles. The results show that no molecule crossover occurred based on absorption spectroscopy measurements (Figures 5 and S5), as the reaction requires. With an instrument detection limit of 0.01 (absorbance) and the molar absorptivity of 9,000 M^{-1} cm^{-1} and 81,000 M^{-1} cm^{-1} for ADPD and Br_2B-OAc, respectively, we estimate a detection limit of 1.11 μM and 0.12 μM. With a cuvette volume of 1.5 mL, the detection limit for ADPD and Br_2B-OAc is 1.67 nmol and 0.18 nmol, respectively. These amounts unable to account for the observed singlet oxygenation. Thus, the data support a reaction in which there is no exchange of compounds between P_{PS} and P_Q particles, whereas $^1O_2$ freely migrates through-space and between the particles.

Control reactions also demonstrated that particle size did not strongly influence the production of $^1O_2$. It is known that particles of different sizes can influence light scattering and this can affect our background signal between samples.[48-50] From our analysis, varying the P_{PS} particles size from an ~70 μm to >800 μm, showed no significant difference in the $^1O_2$ phosphorescence decay curves with τ_{obs1} and τ_{obs2} values of 59 and 542 μs, respectively (See SI experimental details, Figure S4 and Table S1).

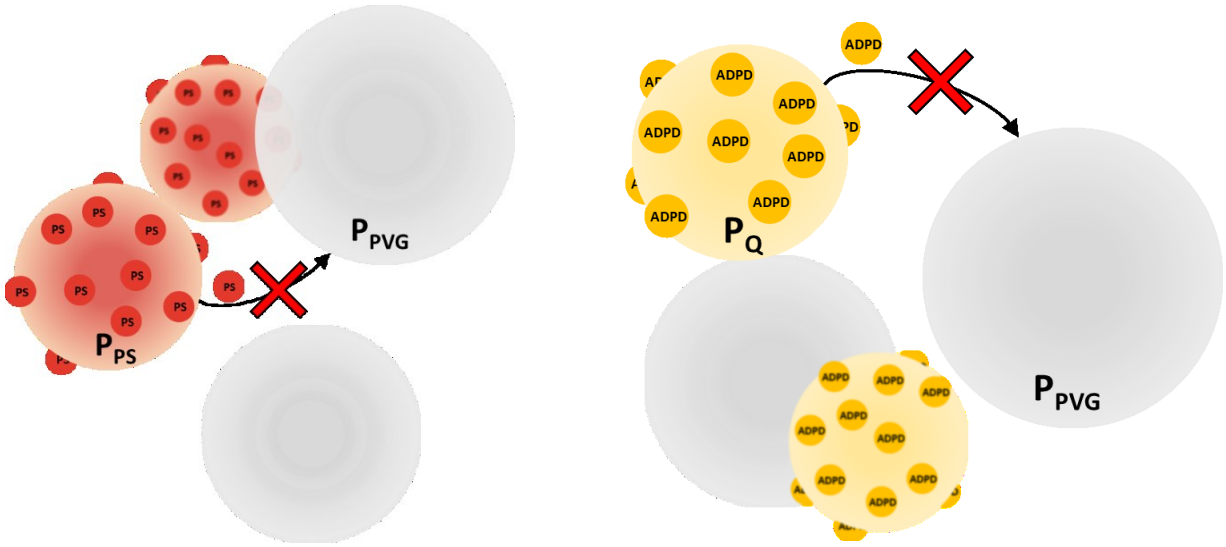

Figure 5. Particles size 38 µm > particle < 100 µm containing the PS (left) or the quencher ADPD (right) were mixed with native particles size 100 µm > particle < 800 µm to evaluate molecules exchange between particles. PS loading: 0.125 µmol/g; ADPD loading: 0.125 µmol/g.

Singlet oxygen quantum yield (Φ_Δ). The Φ_Δ was measured for the P_{PS} particles by monitoring the increase of the $^1O_2$ phosphorescence as a function of the irradiation time. P_{PS} particles were mixed with P_Q particles containing a loading of 50 µmol/g of DMA. As can be observed in Figure 6 and Table S2, the short component (τ_{obs1}) of the phosphorescence decay traces remained similar with the irradiation time. The τ_{obs2} increased by 58% (Table S2) upon 150 s of irradiation with a Nd:YAG laser operating at 532 nm, 10 Hz and 10 mJ/pulse. The increase in the τ_{obs2} from 320 to 550 µs is attributed to the presence of the anthracene (DMA) trapping agent (50 µmol/g) to quench $^1O_2$ in the former. Because anthracene trapping agents are known to mainly quench $^1O_2$ chemically and not physically,[45,47,51,52] the approximate DMA consumption as a function of the irradiation time and particle density permitted conversion of units from µmol/g to molar. Similar to the indirect determination of the Φ_Δ, a pseudo first-order kinetic for this reaction was proposed (eqs S3-S6). Plots of $ln[DMA]_0/[DMA]$ vs irradiation time indicated that the

conversion of DMA followed a pseudo-first order kinetics with the irradiation time (Figure 7). By a linear fit of the data in Figure 7 it was possible to determine the observed rate constant (k_{obs}). Since there is not a k_{obs} value for a photosensitizer in a similar system to be used as a reference, we compared our k_{obs} (8.8×10^{-3} s^{-1}) value with that obtained for Br_2B-OAc in acetonitrile $k_{obs} = 9.0 \times 10^{-3}$ s^{-1}. To determine Φ_Δ in this work, the k_{obs} in solid P_{PS} particles was compared with k_{obs} obtained for the same PS in solution (acetonitrile). Light scattering can be significant in solid samples compared to homogeneous solution, and depends on the refractive index.[53,54] In our case, the Φ_Δ with τ_{obs2} shows little or no effect from scattering unlike τ_{obs1} which shows a pronounced effect from scattering (see section PS loading optimization, above). For example, τ_{obs1} is perturbed by 50%, whereas τ_{obs2} is perturbed by less than 4%. In eq S7, the value for the diffractive index of acetonitrile (1.34)[55] was used for η_{st} (st = acetonitrile standard). Meanwhile, the value for η_{PPS} was considered to be 1.00 and the air/solid Φ_Δ was treated as a standard-like system. The Φ_Δ for the P_{PS} particles was found to be 0.58 and is consistent (~25% smaller) with the previously reported in solution by us and others (0.79).[56] Irradiation of the sample above 150 s resulted in a considerable amount of dye photobleaching, indicated by a significant decrease in the signal intensity (Figure S6). Furthermore, τ_{obs2} plateaus for irradiation periods longer than 120 s (orange trace in Figure 4 and yellow molecules in Figure 5) this can be attributed not only to PS bleaching, but also to complete consumption of the DMA on particles due to airborne $^1O_2$ produced from nearby P_{PS} particles.

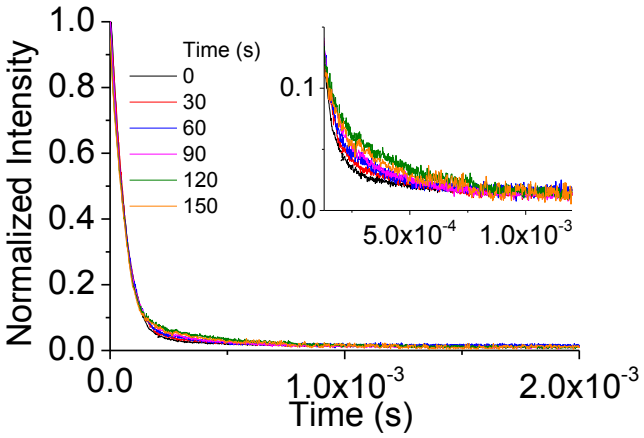

266

267 **Figure 6.** Normalized intensity decay curves of photoexcited mixtures of P_{PS}:P_Q (1:1) particles.
268 The quencher loading was kept constant at 50 μmol/g and the samples were irradiated for
269 different times. P_{PS} = 0.050 μmol/g. Experiments were done in ambient conditions. Inset: zoom-
270 in of the normalized intensity decay curves between 1.3×10^{-4} to 1.2×10^{-3} s showing an intensity
271 enhancement over time.

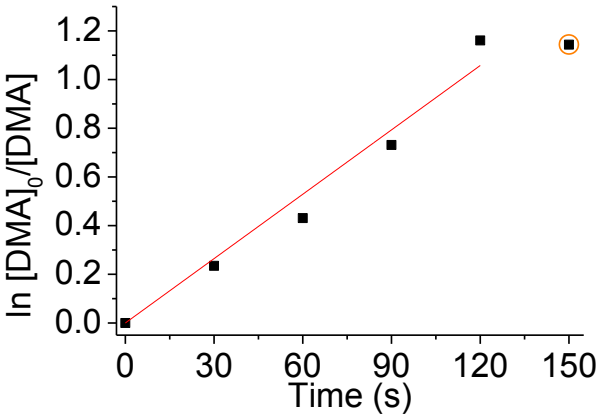

272

273 **Figure 7.** Pseudo first-order kinetic data fitting for the reaction of airborne $^1O_2$ with DMA
274 loaded onto particles [P_{DMA} (50 μmol/g) and P_{PS} (0.050 μmol/g)]. The square highlighted with an
275 orange circle was not included in the fitting and indicates that a plateau was reached after 120 s
276 of irradiation as a result of the consumption of the DMA quencher.

Rate constants for airborne $^1O_2$ quenching by anthracene-coated particles. To gain information on the generation of $^1O_2$ by P_{PS} when exposed to light, we developed a quenching assay that consisted on monitoring the $^1O_2$ phosphorescence intensity decrease upon the loading of the anthracene quencher onto the particles. Quencher particles (P_Q) were prepared by adding two anthracene derivatives: DMA and ADPD (Figure 1). DMA is soluble in organic solvents such as ACN and toluene, while ADPD is water-soluble at basic pH and used as in homogeneous solution,[47,57] but not as $^1O_2$ trapping agents at the air/particle interface as described here. For our experiments, 100 mg of P_{PS} were mixed with 100 mg of P_Q particles containing increasing loadings of the corresponding quencher in an open quartz cuvette.

The $^1O_2$ phosphorescence intensity vs time for different loadings of DMA and ADPD are shown in Figure 8A and 8B, respectively. Figure 8 and Table 3 show the decay for the short component remains constant (~60 μs) in the absence of the anthracene quenchers. Fittings of the data at shorter times scales are shown in Figures S7 and S8 (Supporting Information). This is consistent with $^1O_2$ deactivation by native particles bearing Si–OH groups since $^1O_2$ can undergo quenching via electronic to vibronic (e-to-v) exchange energy transfer from O–H bond oscillators.[58] However, this e-to-v quenching path is not noticeably significant since the addition of native particles do not affect the lifetime of airborne $^1O_2$; for example, τ_{obs2} for P_{PS} (560 μs, Table 2) with the value obtained in Table 3 for a mixture P_{PS}:P_{native} (1:1) (559 μs). There is a significant decrease in τ_{obs2} in the presence of the particles bearing adsorbed anthracene compounds. The lifetime for the long component decreased 1.8 and 1.6 times upon the addition of the P_Q particles of DMA and ADPD, respectively (50 μmol per gram particle).

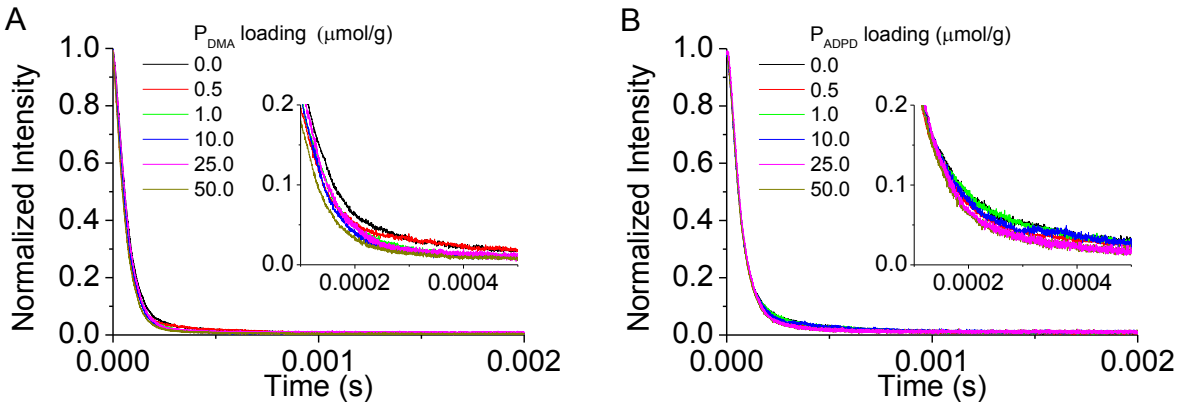

Figure 8. Normalized intensity decay curves of photoexcited mixtures of P_{PS}:P_Q (1:1) particles increasing the quenchers loading of (A) DMA and (B) ADPD. The insets show shorter times scales. The photosensitizer loading for P_{PS} was kept at 0.050 μmol/g. Experiments were done in ambient conditions. Intensity decay was monitored at 1270 nm.

Table 3. Lifetime measurements for singlet oxygen formation and quenching in P_{PS}:P_Q (1:1) particle mixtures.

quencher loading (μmol/g)	**DMA**		**ADPD**	
	τ_{obs1} (μs)[b]	τ_{obs2} (μs)[b]	τ_{obs1} (μs)[b]	τ_{obs2} (μs)[b]
0[a]	60.8	559	59.2	552
0.5	56.6	556	57.6	544
1	57.8	547	58.6	543

10	56.5	493	57.6	502
25	59.1	413	60.3	436
50	57.8	313	59.6	343

[a] P_{PS} particles where mixed with native particles average size (69 μm) in a 1:1 ratio. [b]Errors for the short lifetimes are typically ±1 μs and for the long lifetimes ±5-10 μs; fitting error ranges from 0.01 to 0.03 μs.

The rate constants for deactivation of airborne $^1O_2$ is predicted by eq 1,

$$k_{obs2} = k_d + (ASI\text{-}k_T)\,[Q] \quad (1)$$

and as demonstrated by the plot shown in Figure 9, where $ASI\text{-}k_T$ is the air/solid interface total rate constant of $^1O_2$ by the anthracene trapping agents on adsorbed on the particles, [Q] is the concentration of DMA or ADPD (expressed as μmol of quencher per gram particle), and k_d is the rate constant of deactivation of $^1O_2$ on the particle or in air. $ASI\text{-}k_T$ values for an interparticle or other air/particle configuration have not been reported in the past. These results will provide insights on the efficiency of $^1O_2$ delivery through space and its quenching by compounds at a surface. From the relationship with $1/\tau_{obs2}$, k_{obs2} was obtained and plotted as a function of the anthracene quencher loading (Figure 9A and 9B). Fitting of the data to a straight line gives from the slope $ASI\text{-}k_{T,DMA} = (2.8 \pm 0.8) \times 10^7$ g mol^{-1} s^{-1} ($R^2 = 0.99$) for DMA (Figure 9A), and $ASI\text{-}k_{T,ADPD} = (2.1 \pm 0.9) \times 10^7$ g mol^{-1} s^{-1} ($R^2 = 0.99$) for ADPD (Figure 9B). From the intercept, k_d values (~1.80×10^3 s^{-1}) were obtained indicating a lifetime for airborne $^1O_2$ of 550 μs. A somewhat similar value for gaseous $^1O_2$ (980 μs) in the core of a water bubble was previously measured.[35,36]

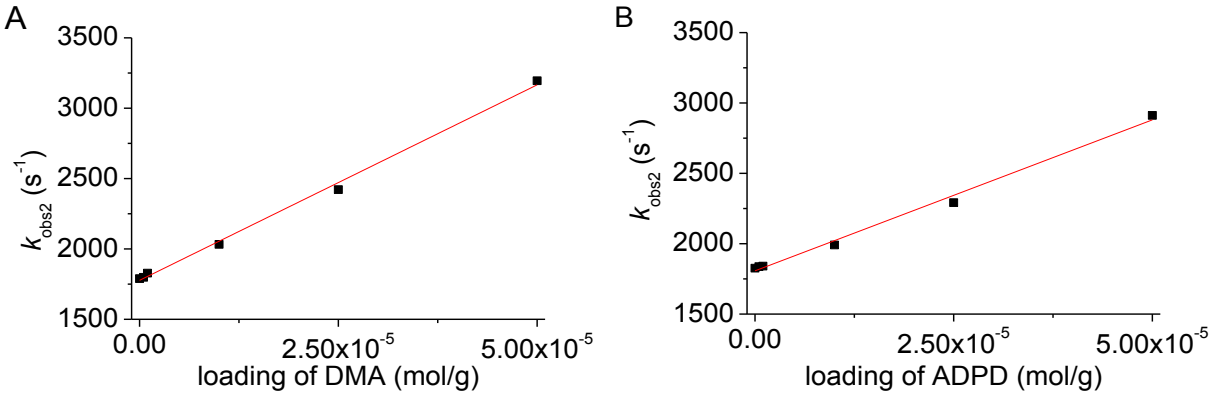

Figure 9. *ASI-*k_T values measured in the interparticle system. Plots of k_{obs2} (s^{-1}) as a function of the mols of quencher adsorbed per gram particle (A) DMA and (B) ADPD. Experiments were performed in ambient conditions.

Mechanism. The above direct-laser detection data provide a strong argument for the mechanism suggested in Figure 2. The data also provide strong evidence for interfacial *and* airborne $^1O_2$, and reactivity of $^1O_2$ at a second particle surface. The $^1O_2$ phosphorescence data show its quenching on the P_{PS} particle surface itself with a short lifetime (~60 μs). Singlet oxygen can transit off the particle and possesses a longer lifetime of ~550 μs as an airborne species. In the absence of particle-coated antracene, a longer lived $^1O_2$ is retained. The Φ_Δ for P_{PS} at the air-solid interface was detemined to be 0.58 by monitoring the increase of τ_{obs2} upon consumption of adjacent particle-adsorbed with DMA. This value was slightly lower than previously reported for the Br_2B-OAc sensitizer and DMA in solution,[56] suggesting that the photophysical properties of the PS to produce $^1O_2$ while adsorbed on particles largely remains intact.

342 The rate constant, k_T, corresponds to the anthracene compound induced total removal of $^1O_2$,
343 which is for the first time measured at the air/particle interface. The quenching effect of $^1O_2$
344 along the particle-adsorbed and airborne pathways are deduced. Clennan et al.[59] have reported
345 heterogenous 2-phase (liquid-solid) k_T values for quenching of $^1O_2$ by modified surfaces of
346 porous silica particles covalently bound to sulfides, where k_T values were between 27.7-29.8 L g^{-1} s^{-1} and "solution-phase like" units of M^{-1} s^{-1} (Table 4). To compare with our results, our *ASI*-k_T
348 values in M^{-1} s^{-1} are based on the density of PVG (δ = 1.38 g/mL).[42] The heterogeneous k_T
349 values are obtained in the order of (1.5-5.2) × 10^4 M^{-1} s^{-1}, suggesting a reduced $^1O_2$ accessibility
350 to the anthracene compound at the interface compared to solution. Furthermore, we validated the
351 measurement of $^1O_2$ quenching by DMA in acetonitrile (9.44 × 10^7 M^{-1} s^{-1}) and by ADPD in
352 D_2O (6.46 × 10^7 M^{-1} s^{-1} at pH = 10) (Figure S9). The k_T values in homogeneous solution gave
353 very similar values to those previously reported.[47,57] Intriguingly, the values measured in solution
354 are of similar magnitude to that reported for $Me_3Si(CH_2)_{l0}SCH_3$ in benzene (k_T = ~3.32 × $l0^7$ M^{-1}
355 s^{-l}) (Table 4). The k_T for sulfides in organic solvents is mostly comprised of physical quenching,
356 but in alcohol solvents or water is mostly chemical quenching.[60] The virtues of using anthracenes
357 are that they are efficient in chemical quenching leading to endoperoxides, and that the
358 air/particle measurements lay a *solid* foundation (pun intended) for a reference point from which
359 to build on.
360
361

362 **Table 4.** Rate constants for total quenching (k_T) of anthracenes and sulfides in solution, at the
363 air/particle interface, or in solution/particle mixtures.

medium	**quencher**	**solvent**	**homogeneous k_T (M^{-1} s^{-1}) × 10^7**
homogeneous solution	DMA	MeCN	(9.44 ± 0.33)[a]
	ADPD	D_2O	(6.46 ± 0.18)[a]
	$Me_3Si(CH_2)_{10}SCH_3$	C_6H_6	3.32[c]

		solid support	**heterogeneous k_T**	**heterogeneous k_T (M^{-1} s^{-1}) × 10^4**
air/particle interface	DMA	particles	(2.8 ± 0.8) × 10^7 g mol^{-1} s^{-1}	2.02[b]
	ADPD	particles	(2.1 ± 0.9) × 10^7 g mol^{-1} s^{-1}	1.56[b]
solution/particle mixture	$ClSiMe_2(CH_2)_{10}SMe$	silica	27.7-29.8 L g^{-1} s^{-1}	4.8-5.2[c]

364 [a]This work. [b]This work with porous Vycor glass particle; conversion using δ_{PVG} = 1.38 g/mL;
365 [c]Reference [59] with a loading of 573 μmol of $ClSiMe_2(CH_2)_{10}SMe$ per gram silica.

366

Technical Implications. The direct-detection particle-air-particle method described here produces $^1O_2$ which transits off the particle and migrates through-air for an oxidation reaction on a second particle surface. The photosensitizer on one particle is physically separated from the antrancene trapping agent on a second particle. Measurements of the total quenching rate constants of $^1O_2$ by surface-adsorbed anthracene traps was developed. The work improves the state of the art by uncovering the mechanistic framework in Figure 2 that increase in anthracene particle loading decreases the airborne $^1O_2$ lifetime, for data that are otherwise challenging to acquire. Attributing the phosphorescence data to $^1O_2$ the air/solid interface and airborne state makes this method advantageous to others, which typically use indirect or EPR trapping in homogeneous solutions or heterogeneous slurries in solution.[61−64] The efficient transfer of $^1O_2$ between particulates as a gaseous species makes this method a relevant model for a natural or artificial air/solid interface and fate of airborne $^1O_2$ damage.

Our 3-phase interparticle reactive oxygen delivery system provides proof of concept for particle sensitization, reactive oxygen transfer in air, and oxidative damage to adjacent solid. This particle-air-particle 3-phase system connects to fields of atmospheric chemistry, environmental chemistry, and photochemistry with surface trapping agents, and also relevance of bi- and triphasic phenomena in $^1O_2$ oxidation chemistry.[34−36,65−68] That the amount of anthracene quencher loaded was linearly dependent, provides a key reference point for compound quenching on environmental surfaces for potential extrapolation, that trapping can increase steeply with loadings of oxophilic traps. We provide mechanistic evidence for the transfer of airborne $^1O_2$ during the photooxidation of anthracene compounds adhered to particles. We reveal through sensitizer particle loading that airborne $^1O_2$ release and transport can be controlled. The acceptor particle is varied with loadings of anthracene trapping agents to offer a way to unveil $^1O_2$

390 quenching on solid surfaces. Now we advance the state of the art with a direct phosphorescence
391 detection technique with a particle-air-particle system, which can set the stage for opening up an
392 area of direct methods on air-solid ROS of importance to environmental chemistry.

393 The results suggest important questions worthwhile of future research. It remains to be tested
394 on how the above "artificial" particles can be compared to natural particles. It is unclear whether
395 low phosphorescence can be observed in airborne $^1O_2$ oxidation of natural particles. Further
396 environmental photochemistry experiments are needed, including sulfide pesticides adsorbed to
397 soil surfaces for determination of $^1O_2$ rate constants. Future work will be required to assess the
398 physical quenching and chemical quenching components at the air/solid interface with
399 compounds. The technique could potentially also be exploited for airborne $^1O_2$ inactivation of
400 soil-bound microbes at air/solid surfaces.

401 We identify $^1O_2$ quenching directly by near-IR phosphorescence in the airborne state and at the
402 air/solid interfaces with k_T measurements of adsorbed trapping agents. These direct detection and
403 particle-induced quenching steps are amenable for further investigation, in atmospheric and
404 particulate processes for singlet oxygen deactivation.

405

406

407 **ASSOCIATED CONTENT**

408 **Supporting Information**

409 Details pertaining the PS loading in PVG particles, computational details, PS-PS distance
410 calculation, $^1O_2$ luminescence validation at 1270 nm, effect of particle size on the production and
411 phosphorescence of $^1O_2$, Interfacial air/solid Φ_Δ, evidence for lack of exchange of PS and ADPD
412 molecules between particles, quenching rate constant of $^1O_2$ by DMA and ADPD in

homogeneous solution, synthesis of Br_2B-OAc, H_2B-OAc, and ADPD, supporting equations S1-S7, supporting Tables S1-S2, supporting Figures S1-S9.

AUTHOR INFORMATION

Corresponding Authors

adurantini@exa.unrc.edu.ar; agreer@brooklyn.cuny.edu

ORCID

Andrés M. Durantini: 0000-0002-7898-4033

Alexander Greer: 0000-0003-4444-9099

Present Addresses

†Author current address: IDAS-CONICET, Departamento de Química, Facultad de Ciencias Exactas, Físico-Químicas y Naturales, Universidad Nacional de Río Cuarto, Ruta Nac. 36 Km 601, X5804BYA Río Cuarto, Córdoba, Argentina.

Author Contributions

The manuscript was written through contributions of both authors. Both authors have given approval to the final version of the manuscript.

ACKNOWLEDGMENT

AMD and AG acknowledge support from the National Science Foundation (CHE-1856765). AMD also acknowledges support from a Fulbright-CONICET fellowship. We thank Leda Lee for help with the graphic arts.

ABBREVIATIONS

PS, photosensitizer; P_{PS}, sensitizer particle; P_Q, quencher particle; *ASI*-k_T, total $^1O_2$ quenching rate constant; Φ_Δ, singlet oxygen quantum yield; PVG, porous Vycor glass; ADPD, 9,10-anthracene dipropionate dianion; DMA, 9,10-dimethylanthracene; $^1O_2$, singlet oxygen; τ_{obs1}, short observed lifetimes; τ_{obs2}, long observed lifetime; k_{obs1}, observed rate constant for singlet oxygen on the surface; k_{obs2}, observed rate constant for airborne $^1O_2$; k_{obs}, observed rate constant of $^1O_2$ quenching by DMA; k_d, is the rate constant of deactivation of $^1O_2$ by the surrounding environment; Q, quencher.

REFERENCES

1. Vione, D.; Maurino, V.; Minero, C.; Pelizzetti, E.; Harrison, M. A. J.; Olariu, R.-I.; Arsene, C., Photochemical Reactions in the Tropospheric Aqueous Phase and on Particulate Matter. *Chem. Soc. Rev.* **2006**, *35*, 441-453.

2. Larson, R. A.; Marley, K. A., Singlet Oxygen in the Environment. In *Environmental Photochemistry*, Boule, P., Ed. Springer: Berlin, 1999; pp. 123-137.

3. Zeng, T.; Arnold, W. A., Pesticide Photolysis in Prairie Potholes: Probing Photosensitized Processes. *Environ. Sci. Technol.* **2013**, *47*, 6735-6745.

4. Gehling, W.; Khachatryan, L.; Dellinger, B., Hydroxyl Radical Generation from Environmentally Persistent Free Radicals (EPFRs) in PM2.5. *Environ. Sci. Technol.* **2014**, *48*, 4266-4272.

5. Braun, A. M.; Frimmel, F. H.; Hoigné, J., Singlet Oxygen Analysis in Irradiated Surface Waters. *Int. J. Environ. Anal. Chem.* **1986**, *27*, 137-149.

6. Partanen, S. B.; Erickson, P. R.; Latch, D. E.; Moor, K. J.; McNeill, K., Dissolved Organic Matter Singlet Oxygen Quantum Yields: Evaluation Using Time-Resolved Singlet Oxygen Phosphorescence. *Environ. Sci. Technol.* **2020**, *54*, 3316-3324.

7. Manfrin, A.; Nizkorodov, S. A.; Malecha, K. T.; Getzinger, G. J.; McNeill, K.; Borduas-Dedekind, N., Reactive Oxygen Species Production from Secondary Organic Aerosols: The Importance of Singlet Oxygen. *Environ. Sci. Technol.* **2019**, *53*, 8553-8562.

8. Erickson, P. R.; Moor, K. J.; Werner, J. J.; Latch, D. E.; Arnold, W. A.; McNeill, K., Singlet Oxygen Phosphorescence as a Probe for Triplet-State Dissolved Organic Matter Reactivity. *Environ. Sci. Technol.* **2018**, *52*, 9170-9178.

9. Hebert, V. R.; Miller, G. C., Depth Dependence of Direct and Indirect Photolysis on Soil Surfaces. *J. Agric. Food Chem.* **1990**, *38*, 913-918.

10. Gohre, K.; Scholl, R.; Miller, G. C., Singlet Oxygen Reactions on Irradiated Soil Surfaces. *Environ. Sci. Technol.* **1986**, *20*, 934-938.

11. Gohre, K.; Miller, G. C., Singlet Oxygen Generation on Soil Surfaces. *J. Agric. Food Chem.* **1983**, *31*, 1104-1108.

12. Monger, C.; Kelly, E., Silica Minerals. In: *Soil Mineralogy with Environmental Applications*, pp. 611-636.

13. Eysel, W., Thermal Analysis in Earth Sciences. *Thermochim. Acta* **1987**, *110*, 495-499.

14. McKeague, J.; Cline, M., Silica in Soil Solutions: I. The Form and Concentration of Dissolved Silica in Aqueous Extracts of Some Soils. *Can. J. Soil Sci.* **1963**, *43*, 70-82.

15. Hans Wedepohl, K., The Composition of the Continental Crust. *Geochim. Cosmochim. Acta* **1995**, *59*, 1217-1232.

16. Kaur, R.; Labins, J. R.; Helbock, S. S.; Jiang, W.; Bein, K. J.; Zhang, Q.; Anastasio, C., Photooxidants from Brown Carbon and Other Chromophores in Illuminated Particle Extracts. *Atmos. Chem. Phys.* **2019**, *19*, 6579-6594.

17. Kaur, R.; Anastasio, C., Light Absorption and the Photoformation of Hydroxyl Radical and Singlet Oxygen in Fog Waters. *Atmos. Environ.* **2017**, *164*, 387-397.

18. Hullar, T.; Magadia, D.; Anastasio, C., Photodegradation Rate Constants for Anthracene and Pyrene Are Similar in/on Ice and in Aqueous Solution. *Environ. Sci. Technol.* **2018**, *52*, 12225-12234.

19. Haag, W. R.; Hoigne, J., Singlet Oxygen in Surface Waters. 3. Photochemical Formation and Steady-State Concentrations in Various Types of Waters. *Environ. Sci. Technol.* **1986**, *20*, 341-348.

20. Scully, F. E.; Hoigné, J., Rate Constants for Reactions of Singlet Oxygen with Phenols and Other Compounds in Water. *Chemosphere* **1987**, *16*, 681-694.

21. Tratnyek, P. G.; Hoigne, J., Oxidation of Substituted Phenols in the Environment: A QSAR Analysis of Rate Constants for Reaction with Singlet Oxygen. *Environ. Sci. Technol.* **1991**, *25*, 1596-1604.

22. Vione, D.; Minella, M.; Maurino, V.; Minero, C., Indirect Photochemistry in Sunlit Surface Waters: Photoinduced Production of Reactive Transient Species. *Chem. Eur. J.* **2014**, *20*, 10590-10606.

23. Fu, H.; Ciuraru, R.; Dupart, Y.; Passananti, M.; Tinel, L.; Rossignol, S.; Perrier, S.; Donaldson, D. J.; Chen, J.; George, C., Photosensitized Production of Atmospherically Reactive Organic Compounds at the Air/Aqueous Interface. *J. Am. Chem. Soc.* **2015**, *137*, 8348-8351.

24. Kautsky, H.; De Bruijn, H., The Explanation of the Inhibition of Photoluminescence of Fluorescent Systems by Oxygen: The Formation of Active, Diffusing Oxygen Molecules by Sensitization. *Naturwissenschaften* **1931**, *19*, 1043-1043.

25. Kautsky, H.; Hirsch, A.; Fesch, R., Energy Transformations on Boundary Surfaces. VIII. The Significance of the Metastable State in Photosensitized Oxidations. *Ber.* **1935**, *68B*, 152-162.

26. Wolf, S.; Foote, C. S.; Rebek, J., Chemistry of Singlet Oxygen. 29. A Specific Three-Phase "Kautsky Test" for Singlet Oxygen. *J. Am. Chem. Soc.* **1978**, *100*, 7770-7771.

27. Ruzzi, M.; Sartori, E.; Moscatelli, A.; Khudyakov, I. V.; Turro, N. J., Time-Resolved EPR Study of Singlet Oxygen in the Gas Phase. *J. Phys. Chem. A* **2013**, *117*, 5232-5240.

28. Naito, K.; Tachikawa, T.; Cui, S.-C.; Sugimoto, A.; Fujitsuka, M.; Majima, T., Single-Molecule Detection of Airborne Singlet Oxygen. *J. Am. Chem. Soc.* **2006**, *128*, 16430-16431.

29. Naito, K.; Tachikawa, T.; Fujitsuka, M.; Majima, T., Real-Time Single-Molecule Imaging of the Spatial and Temporal Distribution of Reactive Oxygen Species with Fluorescent Probes: Applications to TiO_2 Photocatalysts. *J. Phys. Chem. C* **2008**, *112*, 1048-1059.

30. Pitts Jr, J. N.; Khan, A. U.; Smith, E. B.; Wayne, R. P., Singlet Oxygen in the Environmental Sciences. Singlet Molecular Oxygen and Photochemical Air Pollution. *Environ. Sci. Technol.* **1969**, *3*, 241-247.

31. Ogawa, S.; Fukui, S.; Hanasaki, Y.; Asano, K.; Uegaki, H.; Sumiko, F.; Ryosuke, S., Determination Method of Singlet Oxygen in the Atmosphere by Use of α-Terpinene. *Chemosphere* **1991**, *22*, 1211-1225.

32. Suzen, S.; Gurer-Orhan, H.; Saso, L., Detection of Reactive Oxygen and Nitrogen Species by Electron Paramagnetic Resonance (EPR) Technique. *Molecules* **2017,** *22*, 181.

33. Moor, K. J.; Schmitt, M.; Erickson, P. R.; McNeill, K., Sorbic Acid as a Triplet Probe: Triplet Energy and Reactivity with Triplet-State Dissolved Organic Matter via $^1O_2$ Phosphorescence. *Environ. Sci. Technol.* **2019**, *53*, 8078-8086.

34. Aebisher, D.; Bartusik-Aebisher, D.; Belh, S. J.; Ghosh, G.; Durantini, A. M.; Liu, Y.; Xu, Q.; Lyons, A. M.; Greer, A., Superhydrophobic Surfaces as a Source of Airborne Singlet Oxygen through Free Space for Photodynamic Therapy. *ACS Appl. Bio Mater.* **2020**, *3*, 2370-2377.

35. Bartusik, D.; Aebisher, D.; Ghafari, B.; Lyons, A. M.; Greer, A., Generating Singlet Oxygen Bubbles: A New Mechanism for Gas–Liquid Oxidations in Water. *Langmuir* **2012**, *28*, 3053-3060.

36. Bartusik, D.; Aebisher, D.; Lyons, A. M.; Greer, A., Bacterial Inactivation by a Singlet Oxygen Bubbler: Identifying Factors Controlling the Toxicity of $^1O_2$ Bubbles. *Environ. Sci. Technol.* **2012**, *46*, 12098-12104.

37. Clements, P.; Wells, C. H., Soil Sensitised Generation of Singlet Oxygen in the Photodegradation of Bioresmethrin. *Pestic. Sci.* **1992**, *34*, 163-166.

38. Lincoln, R.; Durantini, A. M.; Greene, L. E.; Martínez, S. R.; Knox, R.; Becerra, M. C.; Cosa, G., Meso-Acetoxymethyl Bodipy Dyes for Photodynamic Therapy: Improved

546 Photostability of Singlet Oxygen Photosensitizers. *Photochem. Photobiol. Sci.* **2017**, *16*,
547 178-184.
548 39. Jacob, L. J.; Deigner, H.-P., Chapter 10: Nanoparticles and Nanosized Structures in
549 Diagnostics and Therapy. In: *Precision Medicine*, Deigner, H.-P.; Kohl, M., Eds. Academic
550 Press: 2018, pp. 229-252.
551 40. Medintz, I. L.; Hildebrandt, N., *Fret-Förster Resonance Energy Transfer: From Theory to*
552 *Applications*. John Wiley & Sons: **2013**; pp. 105-163.
553 41. Jones, G. A.; Bradshaw, D. S., Resonance Energy Transfer: From Fundamental Theory to
554 Recent Applications. *Front. Phys.* **2019**, *7*, 1-19.
555 42. Giaimuccio, J.; Zamadar, M.; Aebisher, D.; Meyer, G. J.; Greer, A., Singlet Oxygen
556 Chemistry in Water. 2. Photoexcited Sensitizer Quenching by O_2 at the Water−Porous Glass
557 Interface. *J. Phys. Chem B* **2008**, *112*, 15646-15650.
558 43. Clarkson, R. B.; Turkevich, J., The Adsorption of Oxygen on Porous Vycor Glass by an EPR
559 Technique. *J. Colloid Interface Sci.* **1972**, *38*, 165-171.
560 44. Wilkinson, F.; Helman, W. P.; Ross, A. B., Rate Constants for the Decay and Reactions of
561 the Lowest Electronically Excited Singlet State of Molecular Oxygen in Solution. An
562 Expanded and Revised Compilation. *J. Phys. Chem. Ref. Data* **1995**, *24*, 663-677.
563 45. Lindig, B. A.; Rodgers, M. A. J., Rate Parameters for the Quenching of Singlet Oxygen by
564 Water-Soluble and Lipid-Soluble Substrates in Aqueous and Micellar Systems. *Photochem.*
565 *Photobiol.* **1981**, *33*, 627-634.
566 46. Aebisher, D.; Zamadar, M.; Mahendran, A.; Ghosh, G.; McEntee, C.; Greer, A., Fiber-Optic
567 Singlet Oxygen [$^1O_2$ ($^1\Delta_g$)] Generator Device Serving as a Point Selective Sterilizer.
568 *Photochem. Photobiol.* **2010**, *86*, 890-894.

569 47. Lindig, B. A.; Rodgers, M. A. J.; Schaap, A. P., Determination of the Lifetime of Singlet
570 Oxygen in Water-d_2 Using 9,10-Anthracenedipropionic Acid, a Water-Soluble Probe. *J. Am.*
571 *Chem. Soc.* **1980**, *102*, 5590-5593.
572 48. Evstrapov, A.; Esikova, N.; Antropova, T., Study of Porous Glasses by the Methods of
573 Optical Spectroscopy. *J. Opt. Technol.* **2008**, *75*, 266-270.
574 49. Ogawa, S., $1/\lambda^4$ Scattering of Light During the Drying Process in Porous Vycor Glass with
575 Nano-Sized Pores. *J. Opt. Soc. Am. A* **2013**, *30*, 154-159.
576 50. Aragon, S.; Pecora, R., Theory of Dynamic Light Scattering from Polydisperse Systems. *J.*
577 *Chem. Phys.* **1976**, *64*, 2395-2404.
578 51. Griesbeck, A. G.; Uhlig, J.; Sottman, T.; Belkoura, L.; Strey, R. Singlet Oxygen
579 Photooxygenation in Water/Pluronic F127 Hydrogels: Increased Reaction Efficiency
580 Coupled with a Switch in Regioselectivity. *Chem. Eur. J.* **2012**, *18*, 16161-16165.
581 52. Fudickar, W.; Linker, T., Theoretical Insights into the Effect of Solvents on the [4 + 2]
582 Cycloaddition of Singlet Oxygen to Substituted Anthracenes: A Change from a Stepwise
583 Process to a Concerted Process. *J. Phys. Org. Chem.* **2019**, *32*, e3951.
584 53. Han, X.; Shen, J.; Yin, P.; Hu, S.; Bi, D., Influences of Refractive Index on Forward Light
585 Scattering. *Opt. Commun.* **2014**, *316*, 198-205.
586 54. Cardona, M.; Merlin, R., Light Scattering in Solids IX. Springer: 2006, pp. 1-14.
587 55. An, N.; Zhuang, B.; Li, M.; Lu, Y.; Wang, Z.-G., Combined Theoretical and Experimental
588 Study of Refractive Indices of Water–Acetonitrile–Salt Systems. *J. Phys. Chem. B* **2015**,
589 *119*, 10701-10709.
590 56. Durantini, A. M.; Greene, L. E.; Lincoln, R.; Martinez, S. R.; Cosa, G., Reactive Oxygen
591 Species Mediated Activation of a Dormant Singlet Oxygen Photosensitizer: From

592 Autocatalytic Singlet Oxygen Amplification to Chemicontrolled Photodynamic Therapy. *J*
593 *Am Chem Soc* **2016**, *138*, 1215-25.
594 57. Günther S., G.; Lemp M., E.; Zanocco, A. L., On the Use of 9,10-Dimethylanthracene as
595 Chemical Rate Constant Actinometer in Singlet Molecular Oxygen Reactions. *J. Chil.*
596 *Chem. Soc.* **2000**, *45*, 637-644.
597 58. Schweitzer, C.; Schmidt, R., Physical Mechanisms of Generation and Deactivation of Singlet
598 Oxygen. *Chem. Rev.* **2003**, *103*, 1685-1758.
599 59. Clennan, E. L.; Chen, M. F., Photooxidation Kinetics in Heterogeneous Media. *J. Org.*
600 *Chem.* **1995**, *60*, 6004-6005.
601 60. Clennan, E. L.; A. Greer, A. The Effect of Alcohols on the Photooxidative Behavior of
602 Diethylsulfide. *J. Org. Chem.* **1996**, *61*, 4793-4797.
603 61. Forbes, M. D.; Ruberu, S. R.; Dukes, K. E., Dynamics of Spin-Polarized Radical Pairs at the
604 Solid/Solution Interface. *J. Am. Chem. Soc.* **1994**, *116*, 7299-7307.
605 62. Forbes, M. D.; Dukes, K. E.; Myers, T. L.; Maynard, H. D.; Breivogel, C. S.; Jaspan, H. B.,
606 Time-Resolved Electron Paramagnetic Resonance Spectroscopy of Organic Free Radicals
607 Anchored to Silica Surfaces. *J. Phys. Chem.* **1991**, *95*, 10547-10549.
608 63. Tarasov, V. F.; Jarocha, L. E.; Avdievich, N. I.; Forbes, M. D., TREPR Spectra of Micelle-
609 Confined Spin Correlated Radical Pairs: I. Molecular Motion and Simulations. *Photochem.*
610 *Photobiol. Sci.* **2014**, *13*, 439-453.
611 64. DeHaven, B. A.; Tokarski, J. T.; Korous, A. A.; Mentink-Vigier, F.; Makris, T. M.; Brugh,
612 A. M.; Forbes, M. D. E.; van Tol, J.; Bowers, C. R.; Shimizu, L. S. Endogenous Radicals of
613 Self-assembled Benzophenone Bis-urea Macrocycles: Characterization and Application as a

614 Polarizing Agent for Solid-state DNP MAS NMR spectroscopy. *Chem. Eur. J.* **2017**, *23*,
615 8315-8319.
616 65. Wang, K.-K.; Song, S.; Jung, S.-J.; Hwang, J. W.; Kim, M.-G.; Kim, J.-H.; Sung, J.; Lee, J.-
617 K.; Kim, Y.-R., Lifetime and Diffusion Distance of Singlet Oxygen in Air under Everyday
618 Atmospheric Conditions. *Phys. Chem. Chem. Phys* **2020**, 22, 21664-21671.
619 66. Sunday, M. O.; Takeda, K.; Sakugawa, H., Singlet Oxygen Photogeneration in Coastal
620 Seawater: Prospect of Large-Scale Modeling in Seawater Surface and Its Environmental
621 Significance. *Environ. Sci. Technol.* **2020**, *54*, 6125-6133.
622 67. Sunday, M. O.; Sakugawa, H., A Simple, Inexpensive Method for Gas-Phase Singlet Oxygen
623 Generation from Sensitizer-Impregnated Filters: Potential Application to Bacteria/Virus
624 Inactivation and Pollutant Degradation. *Sci. Total Environ.* **2020**, *746*, 141186.
625 68. Klaper, M.; Linker, T., Intramolecular Transfer of Singlet Oxygen. *J. Am. Chem. Soc.* **2015**,
626 *137*, 13744-13747.
627